

Article

Performance Analysis of a Double Pass Solar Air Thermal Collector with Porous Media Using Lava Rock

Amar Fahmi Ismail ¹, Ag Sufiyan Abd Hamid ^{2,*} , Adnan Ibrahim ^{1,*} , Hasila Jarimi ¹ and Kamaruzzaman Sopian ¹

¹ Solar Energy Research Institute, Universiti Kebangsaan Malaysia, Bangi 43600, Selangor, Malaysia; p103527@siswa.ukm.edu.my (A.F.I.); hasila.jarimi@ukm.edu.my (H.J.); ksopian@ukm.edu.my (K.S.)

² Faculty of Science and Natural Resources, Universiti Malaysia Sabah, Kota Kinabalu 88400, Sabah, Malaysia

* Correspondence: pian@ums.edu.my (A.S.A.H.); iadnan@ukm.edu.my (A.I.)

Abstract: This paper investigates double-pass solar air thermal collectors with lava rock as the porous media. The addition of lava rock serves as short-term sensible thermal storage for a solar drying system. It also enhances the convective heat transfer rate to the airflow due to an increased heat transfer area and increased turbulence in the air channel. A mathematical model was developed based on energy balance equations and was numerically solved in MATLAB. The collector's thermal performance was studied at various levels of solar intensity and at different wind speeds for different design parameters: collector size, air mass flow rate, and lava rock volume. From the study, the optimum efficiencies that were obtained in the range between the intensities of 500 W/m² and 800 W/m² were 62% to 64%, respectively, with an optimum flow rate of 0.035 kg/s. The optimum porosity of about 89% was selected for the collector by considering the pressure drop and thermal efficiency. An optimal temperature output range between 41.7 °C and 48.3 °C could be achieved and was suitable for agricultural and food drying applications. Meanwhile, compared to conventional DPSAHs, the average percentage increase in the output temperature of the DPSAH with lava rock was found to be higher by 17.5%.

Keywords: solar collector; double pass solar air heater; porous media; packed bed; porous material



Citation: Ismail, A.F.; Abd Hamid, A.S.; Ibrahim, A.; Jarimi, H.; Sopian, K. Performance Analysis of a Double Pass Solar Air Thermal Collector with Porous Media Using Lava Rock. *Energies* **2022**, *15*, 905. <https://doi.org/10.3390/en15030905>

Academic Editors: Pedro Dinis Gaspar

Received: 17 November 2021

Accepted: 28 December 2021

Published: 26 January 2022

Publisher's Note: MDPI stays neutral with regard to jurisdictional claims in published maps and institutional affiliations.



Copyright: © 2022 by the authors. Licensee MDPI, Basel, Switzerland. This article is an open access article distributed under the terms and conditions of the Creative Commons Attribution (CC BY) license (<https://creativecommons.org/licenses/by/4.0/>).

1. Introduction

Fossil fuels that are finite and damaging to the environment necessitate the implementation of alternative energy strategies. As a result, the scientific community has focused on systems that can utilize and transform renewable energy sources, notably solar radiation, into useful energy in recent decades. A solar thermal collector comprising a heat exchanger can convert solar radiant energy into useful thermal energy via the use of a working fluid or a heat transfer fluid such as air or liquid [1–3]. Solar thermal collectors come in two varieties: air and water. Solar thermal air collectors are less attractive than solar thermal water collectors due to their lower thermal efficiency [4]. Solar collectors are commonly employed in low- to medium-temperature applications, including room heating [5], crop drying [6], wood flavoring [7], and other industrial uses. Conventional solar air collectors have low thermal efficiency due to the significant heat loss that occurs between the absorption plate and the moving air stream and a low convective heat transfer coefficient [8]. The heat transfer rate of a solar air collector may increase to improve its thermal performance. With that, various designs and flow patterns have been investigated by researchers in order to increase the thermal performance of conventional solar air collectors, with one strategy being the use of multi-pass air channels. Compared to a single-pass, a double-pass solar air heater (DPSAH) is better than a single-pass solar air heater [9]. In a DPSAH, the heat transfer area is increased to double while keeping the system at a low cost.

To further enhance the performance of a DPSAH, a porous and packed-bed heat transfer enhancement has been introduced by researchers. The packed bed in the DPSAH

serves two main functions. First, due to the immense heat transfer area and high turbulence, porous media will increase the convective heat transfer rate in the air channel. Second, the packed bed serves as short-term sensible heat storage that enables continuous drying, even at low solar irradiance [10]. K. Sopian et al. discovered that the thermal efficiency of an enhanced DPSAH was high compared to a conventional DPSAH [11]. Later, they investigated a DPSAH with porous materials and demonstrated the thermal efficiency of a double-pass SAH with a porous material could achieve efficiencies of 60% to 80% [12]. Compared to a DPSAH without porous materials, the productivity of a DPSAH with porous materials is 20% to 70% higher. The use of porous material in a single-pass and double-pass system was studied by Aldabbagh et al. [13], and is presented in Figure 1.

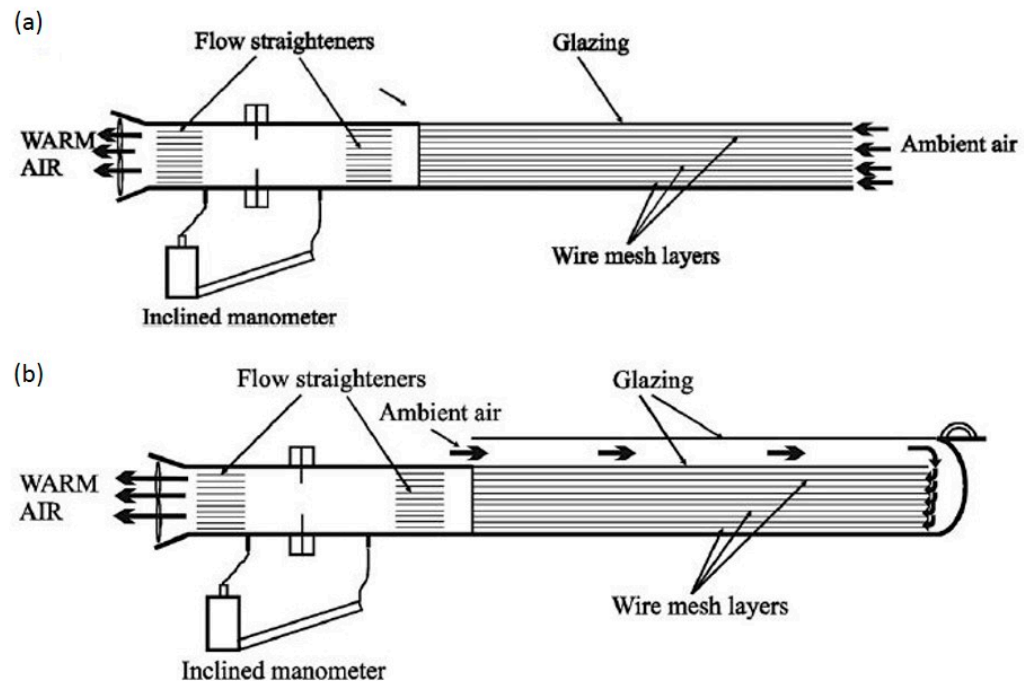


Figure 1. Schematic diagram of (a) a single-pass and (b) double-pass solar air heater with a packed bed [13].

Mahmood et al. examined the behavior of porous media in a single-pass and double-pass air channel, with the highest efficiency that was achieved being 54.74% [9]. In the study by Roy et al., the thermal performance of a DPSAH was improved by replacing square-shaped steel wire mesh in the second channel [14]. In their study, the highest efficiency achieved was 82.20%. Glass spheres were employed as porous media in the research by Ahmed and Mohammed [15]. The obtained thermal efficiencies were 89.52% and 75% in structures with and without porosity. Monem et al. investigated a DPSAH using black-coated wire mesh as a packed bed on the absorbing plate [16] with a porosity of 83% and with a different mass flow rate between 0.0115–0.038 kg/s. They concluded that the efficiency of a DPSAH using black-coated wire mesh as a packed bed was 22% higher than without wire mesh. In the experimental study developed by Singh et al., ten successive wire meshes were placed in the second air channel of a DPSAH between converging fins at an 11° tilt [17]. The optimum value of the mass flow rate for the best thermal presentation of the solar air heater was found to be 0.023 kg/s.

Advancements are made regularly in numerical fields of study, whether in mathematics, design, or the application of formulae in heat transfer analysis. According to [18], V-corrugated mesh is the best alternative. They claimed that a larger channel length produces faster heat retention rates, reducing the SAH's top heat loss. Dissa et al. [19] assessed the efficacy of porous and non-porous compound absorbers made of corrugated iron sheets and aluminum mesh. The efficiency that was gained during the unstable phase was be-

tween 18 and 61%, while the efficiency that was obtained during the partial condition process ranged between 37% and 61% for the theoretical and practical investigation of a two-pass packed-bed SAH with a recycling ratio of 1.5 [20]. The wire mesh layers that had placed on the absorber plate increased the temperature of the airflow, hence raising the recycle ratio as the heat removal percentage grew. In comparison, when the mass flow rate of the air increases, the air temperature decreases. At a mass flow rate of 0.025 kg/s and a recycling ratio of 1.5, a maximum thermal efficiency of 70% was reached. Singh and Dhiman built a packed-bed recycling flow in which the output air from the second duct was directed to the input of the third duct [21]. They discovered that a recycling ratio of 1.8 and mass flow rates ranging from 0.01 to 0.02 kg/s resulted in higher thermal efficiency. Double-pass SAHs both with and without metal matrix porous media were numerically analyzed. According to the researchers, reduced porosity results in increased thermal efficiency, while increased porosity results in a reduced pressure drop. Thermal efficiency was enhanced by 20% and 17%, respectively, when the porosity was 90% and 97.5% [22]. Using experimental and Computational Fluid Dynamic (CFD) simulations, the thermal performance of indirect sun dryers with mesh absorbers was compared to solar dryers without mesh configuration. The study used Pepino fruits with thicknesses of 3 mm and 5 mm, and four experiments were set up using two different dryers. The collector efficiencies were 72.15% and 70.60%, respectively, when using a normal drier with 3 mm and 5 mm thick fruits. The collector efficiencies were 78.06% and 80.39%, respectively, when using drier mesh absorbers with 3 mm and 5 mm holes. In terms of enhanced food quality, the overall average drier efficiency of an indirect dryer that had undergone mesh absorber modifications was 23.08% [23]. Singh [24] extended the work numerically and experimentally by utilizing serpentine wavy wire mesh to improve the thermal performance of the DPSAH. They conducted computational CFD studies that were capable of elucidating the physics of the flow-through a porous 85–95% wire mesh wavy serpentine solar air heater at mass flow rates ranging from 0.01 kg/s to 0.05 kg/s. They also optimized the thermal performance of the porosity of the solar air heater's wire mesh. At a mass flow rate of 0.04 kg/s, the DPSAH had an efficiency of 80%. They determined that thermohydraulic efficiency improves with the mass flow rate and eventually becomes negligible at a mass flow rate that is more than 0.03 kg/s. Those wavy layers absorb more of the heat transfer area than flat plates do. Tables 1 and 2 show the summary of different types of porous materials that have been used as a packed bed for both experimental and numerical analyses.

Table 1. Summary of different types of porous materials as the packed bed.

Author	Year	Type of Porous Material
Mahmood et al. [9]	2015	Wire mesh
Roy et al. [14]	2017	Square shape steel wire mesh
Ahmed and Mohammed [15]	2017	Glass Sphere
Monem et al. [16]	2019	Black coated wire mesh
Singh et al. [17]	2019	Ten successive wire mesh

Table 2. Summary of different types of porous materials in numerical studies.

Author	Year	Type of Porous Material
Velmurugan and Kalaivanan [18]	2015	V-corrugated shaped wire mesh
Dissa et al. [19]	2016	corrugated iron sheet and mesh of aluminum
Singh and Dhiman [20]	2016	Wire mesh
Singh and Dhiman [21]	2018	Wire mesh
Hernández et al. [22]	2019	Porous matrix (in contact with absorber plate)
Güler et al. [23]	2020	Iron wire mesh
Singh [24]	2020	Serpentine wavy wire mesh

Setting it apart from previous research, this paper investigates the potential of lava rock as the porous media to enhance the heat transfer rate in DPSAH while serving as the short-term sensible heat storage method for a solar collector that is suitable for food drying applications. The use of lava rock as a porous material is new and has never been investigated by other researchers in related fields. Additionally, unlike a conventional DPSAH, which commonly employs metal mesh wire, lava rock has the following key advantages; first, metal mesh carryover, which can be hazardous to the food being dried, can be avoided; second, metal corrosion is not an issue; and finally, lava rock is, in general, a safe organic material that has been widely used for domestic applications, such as in barbeque grills. The design of a DPSAH with lava rock is discussed in this research and contributes to the study of double-pass solar air heating applications. In addition, a DPSAH using lava rock is compared to conventional DPSAHs in terms of solar drying performance in order to demonstrate its potential.

2. Research Methodology

The research methodology approach is divided into four key stages. The first stage is the development of the design of the double-pass solar thermal collector with a porous material. Here, the proposed design concept is detailed, and the selection of the porous material is justified. The second stage involves heat transfer analysis and mathematical model development in transient analysis using energy balance equations. Next, the model is validated against established experimental results. Finally, to investigate the collector's performance, a computer simulation was performed in MATLAB using the validated mathematical model to assess the collector's performance.

2.1. Design Concept

In this study, we investigated a double-pass solar air heater (DPSAH) using lava rock as a porous material that has been placed in the second channel (see Figure 2). The double-pass collector consists of two air channels; the first channel is constructed between the glass cover and the absorber plate. Meanwhile, the second air channel, which flows in the reverse direction, is created between the absorber plate cover and the backplate. The lava rock is placed in the second air channel as a heat storage material and as a heat transfer enhancement technique for the working fluid, air. The size of the collector is 54 cm wide, 240 cm long with an upper channel depth of 3.5 cm and of 7 cm for the bottom channel. A material called insuflex with a thickness of 5 cm to avoid heat loss dissipation was selected as the insulation cover. Some of the geometrical, thermal, and physical values that were used to optimize fabrication are listed in Table 3. This numerical study uses lava rock, which is also known by its scientific name vesicular basalt, images of which are presented in Figure 3. The rock is also known as scoria rock and is formed from a volcanic eruption and is generally black or red. Lava rock is widely used in the construction of buildings, landscaping, or barbeque grills due to the following reasons [25–27]:

- It has high porosity;
- It has a low density;
- It has high moisture absorption;
- It has a high heat capacity (capability to retain heat).

Table 3. The geometrical, thermal, and physical values.

Parameters	Numerical Values
The volume of lower channel, V_1 (m^3)	0.09
Ambient temperature, T_a (K)	298.15
Inlet air temperature, T_i (K)	300.15
Mass Flow rate, (kg/s)	0.015, 0.02, 0.025, 0.03, 0.035, 0.04, 0.045, 0.05, 0.055, 0.06, 0.065

Table 3. Cont.

Parameters	Numerical Values
Solar Irradiance, W/m^2	500, 600, 700, 800
The transmittance of glass, τ_g	0.80
Absorption of glass, α_g	0.05
Absorption of the plate, α_p	0.95
An emissivity of glass, ε_g (Low emissivity coated glass)	0.35
An emissivity of the absorber plate, ε_p	0.9
An emissivity of the bottom plate, ε_b	0.86
An emissivity of porous material, ε_{pm}	0.93
Sigma, σ	5.670×10^{-8}
Thermal conductivity of insulation, $\frac{W}{m^2}$	0.038
Thermal conductivity of porous, $\frac{W}{m^2}$ [28]	1.56
Specific heat capacity of porous, $\frac{J}{kgK}$ [28]	1200
The density of porous material, ρ_m [28]	2600
Wind velocity, V_w , m/s	1

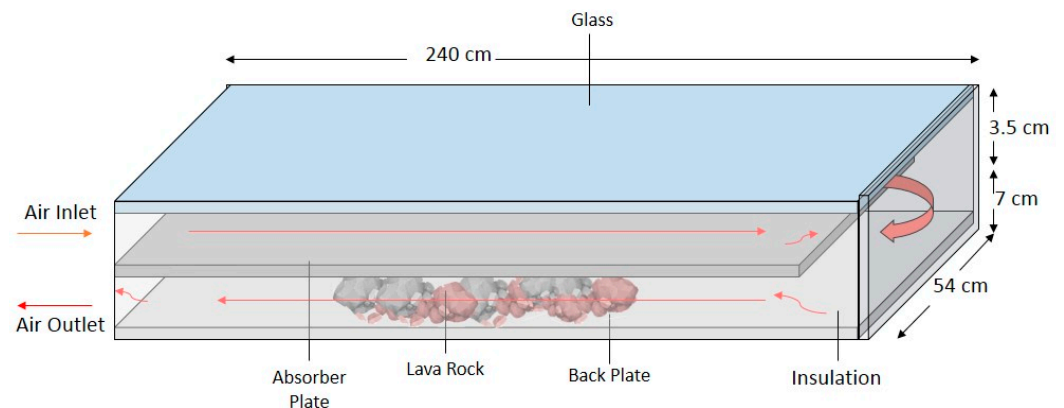


Figure 2. Cross-section of double pass solar air heater (DPSAH) with lava rock.

2.2. Mathematical Model Using the Energy Balance Method

The heat transfer mechanism that takes place in the solar collector is presented in Figure 4. There are six layers that must be considered when calculating the heat transfer in the energy balance: the glass's surface, the first and the second air paths, the surface of the absorber plate, the lava rock, and the insulation layer. In order to determine how much solar radiation is absorbed by the atmosphere, an energy balance is used. The energy balance equations for the DPSAH with lava rock were generated using transient one-dimensional energy balances.

The following assumptions can be made to simplify the analysis:

- The analysis is 1-dimensional;
- The heat capacity of glass, absorber plate, and back surface is negligible;
- Only the heat capacity of the porous material is considered in the transient analysis;
- The thermal resistance of the glass cover and the backplate are assumed to be negligible.

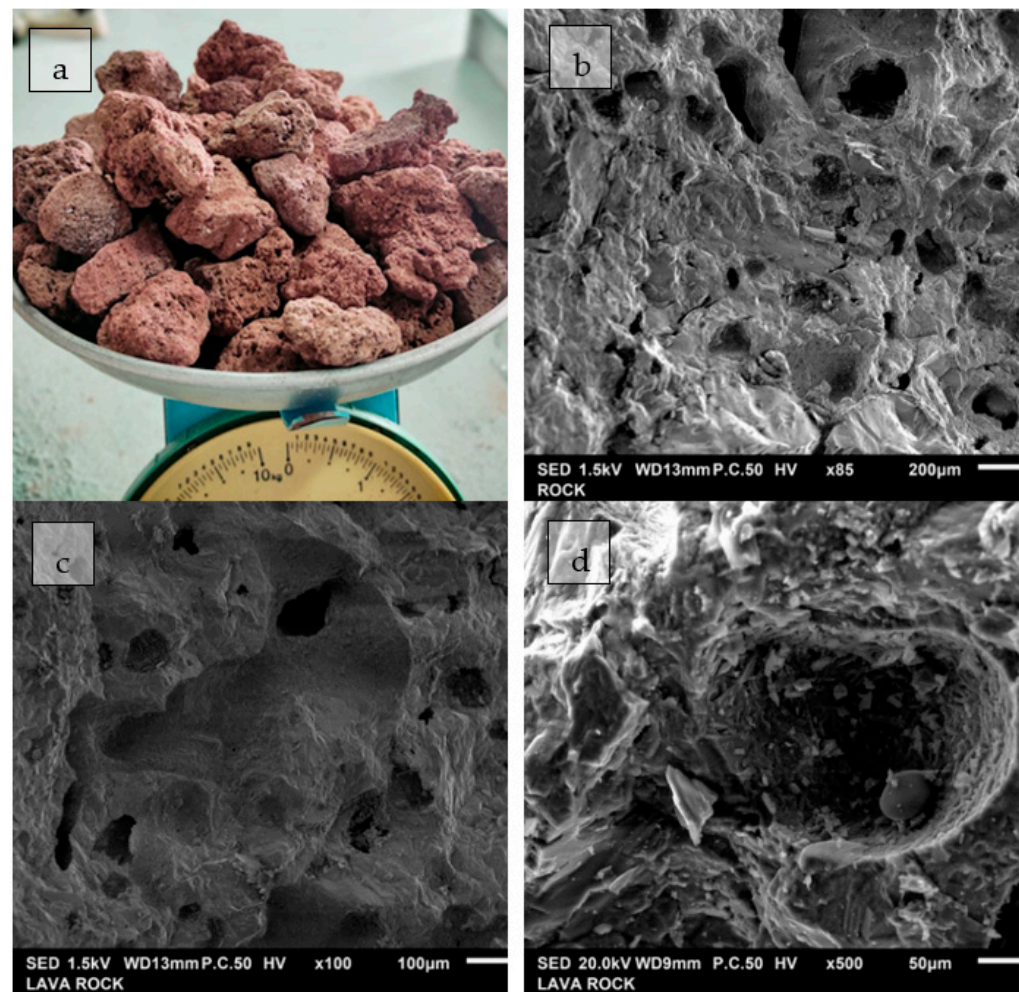


Figure 3. (a) Images of lava rock (Scoria type) ready for installation, (b–d) Scanning Electron Diffraction (SED) images of the lava rock (Scoria type) under different magnification showing the porosity of the rock.

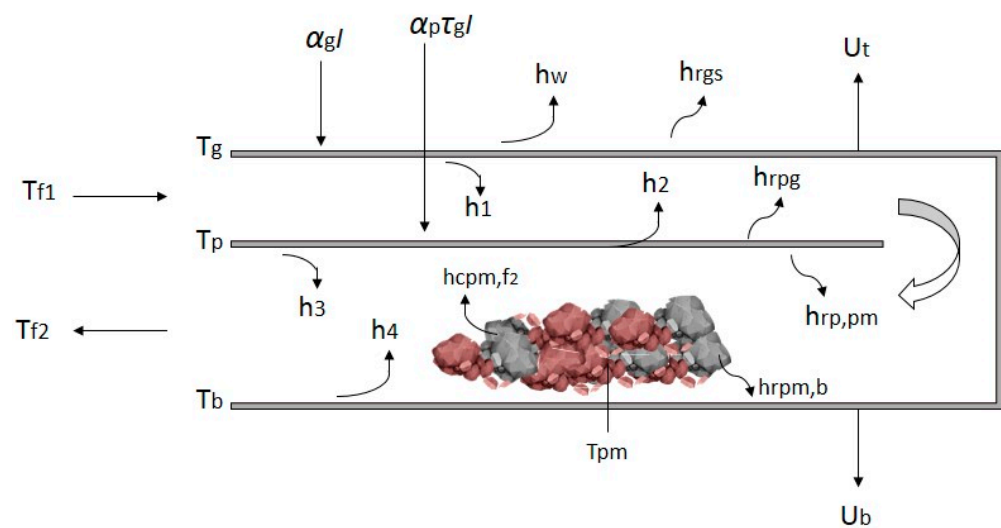


Figure 4. Schematic of heat transfer coefficient in DPSAH with lava rock.

The energy balance equations for each of the collector’s components are as follows:

For the glass cover component:

$$\alpha_g I + h_{rpg}(T_p - T_g) = U_t(T_g - T_a) + h_1(T_g - T_{f1}) \quad (1)$$

(1a) (1b) (1c) (1d)

The terminologies for heat transfer are as follows:

(1a): The rate of the solar energy received by the glass cover per unit area. (1b): The rate of heat transfer between the absorber plate and the glass cover. (1c) The top heat rate-lost to the atmosphere per unit area. (1d): The rate of convective heat transfer from the inner surface of the glass cover to the heat transfer fluid in the first air channel.

For the heat transfer fluid in the first air channel:

$$Q_1 = h_1(T_g - T_{f1}) + h_2(T_p - T_{f1}) \quad (2)$$

(1e) (1d) (1f)

The terminologies for heat transfer are as follows:

(1e): The heat transfer fluid removes the useful energy in the first air channel. (1f): The rate of heat transfer by convection from the absorber plate to the working fluid in the first air channel:

For the absorber plate:

$$\alpha_p \tau_g I = h_{rpg}(T_p - T_g) + h_2(T_p - T_{f1}) + h_3(T_p - T_{f2}) + h_{rp,pm}(T_p - T_{pm}) \quad (3)$$

(1g) (1b) (1f) (1h) (1i)

The terminologies for heat transfer are as follows:

(1g): The rate of the solar energy absorbed by the absorber plate after transmission through the glass cover (1h): Convective heat transfer from the absorber plate to the working fluid in the second air channel. (1i): Heat transfer via radiation from the absorber plate to the porous material

For the airflow in the second air channel:

$$Q_2 = h_3(T_p - T_{f2}) + h_4(T_b - T_{f2}) + \frac{h_{cpmf2} A_m}{A_c} (T_{pm} - T_{f2}) \quad (4)$$

(1j) (1h) (1k) (1l)

The terminologies for heat transfer are as follows:

(1j): The heat transfer fluid removes the useful energy in the second air channel. (1k): Heat transfer from the surface of the back panel to the airflow in the second air channel via convection. (1l): Heat transfer via convection from the porous material to the airflow in the second air channel.

For the porous materials:

$$h_{rp,pm}(T_p - T_{pm}) = \frac{h_{cpmf2} A_m}{A_c} (T_{pm} - T_{f2}) + k_{pm} \delta_{pm} \frac{\partial^2 T_{pm}}{\partial x^2} + h_{rpm,b}(T_{pm} - T_b) + \frac{M_m C_m A_{pm}}{A_c} \frac{dT_{pm}}{dt} \quad (5)$$

(1i) (1l) (1m) (1n) (1o)

The terminologies for heat transfer are as follows:

(1m): The conductive heat transfer on the x-axis in the porous material. (1n): Radiative heat exchange between the porous materials and the inner surface of the back panel. (1o): The rate of heat stored by the lava rock.

$$h_{rpm,b}(T_{pm} - T_b) = h_4(T_b - T_{f2}) + U_b(T_b - T_a) \quad (6)$$

(1n) (1k) (1p)

The terminologies for heat transfer are as follows:

(1p): The heat loss to the atmosphere through the back panel (insulation layer). The top loss and bottom loss coefficients are calculated using Equations (7) and (8), respectively, where k_t is the thermal conductivity of insulation, and l_t refers to the thickness of the rear insulation.

The radiative and convective heat transfer coefficients are computed according to Equations (9) and (10):

$$U_t = h_w + h_{rgs} \quad (7)$$

$$U_b = \frac{k_t}{l_t} \quad (8)$$

$$h_w = 2.8 + 3.3V_w \quad (9)$$

h_w is the convective heat transfer coefficient due to wind [29], and V_w is the wind velocity.

$$h_{rgs} = \frac{\sigma \varepsilon_g (T_g + T_s) (T_g^2 + T_s^2) (T_g - T_s)}{T_g - T_a} \quad (10)$$

As stated in Equation (10), h_{rgs} is the radiative heat transfer from the glass to the sky, where T_s is the sky temperature given by [30]:

$$T_s = 0.0552T_a^{1.5} \quad (11)$$

The radiative heat transfer between the plate, backplate, and the packed bed can be written using Equations (12)–(14):

$$h_{rpg} = \frac{\sigma (T_p + T_g) (T_p^2 + T_g^2)}{\frac{1}{\varepsilon_p} + \frac{1}{\varepsilon_g} - 1} \quad (12)$$

$$h_{rpb} = \frac{\sigma (T_p + T_b) (T_p^2 + T_b^2)}{\frac{1}{\varepsilon_p} + \frac{1}{\varepsilon_b} - 1} \quad (13)$$

$$h_{rp,pm} = \frac{\sigma (T_p + T_{pm}) (T_p^2 + T_{pm}^2)}{\frac{1}{\varepsilon_p} + \frac{1}{\varepsilon_{pm}} - 1} \quad (14)$$

The energy for the first channel, Q_1 , and the second channel, Q_2 , are defined in Equations (15) and (16), respectively:

$$Q_1 = 2 \dot{m} C_{f1} (T_{f1,o} - T_{f1,i}) / WL \quad (15)$$

$$Q_2 = 2 \dot{m} C_{f2} (T_{f2,o} - T_{f1,o}) / WL \quad (16)$$

The convective heat transfer coefficients due to airflow in the channels can be described using the relationships in Equation (17), where Nu is the Nusselt number, and where D_h is the equivalent diameter:

$$h = \frac{k}{D_h} Nu \quad (17)$$

The laminar flow region, the Nusselt number for ($Re < 2300$), is proposed by [31]:

$$Nu = 5.4 + \frac{0.00190 \left[RePr \left(\frac{D_h}{L} \right) \right]^{1.71}}{1 + 0.00563 \left[RePr \left(\frac{D_h}{L} \right) \right]^{1.71}} \quad (18)$$

For the transition flow region ($2300 < Re < 6000$):

$$Nu = 0.116 \left(Re^{\frac{2}{3}} - 125 \right) Pr^{\frac{1}{3}} \left[1 + \left(\frac{D_h}{L} \right)^{\frac{2}{5}} \right] \left(\frac{\mu}{\mu_w} \right)^{0.14} \quad (19)$$

The turbulent flow equation is shown in Equation (20) and was derived by Gnielinski [32] using the correlation of the friction factor in Equation (21) determined by Blasius and as mentioned in [33]. The turbulent flow region ($Re > 6000$) can be calculated as:

$$Nu = \frac{\left(\frac{f}{8}\right) Re Pr}{1.07 + 12.7 \left(\frac{f}{8}\right)^{1/2} (Pr^{2/3} - 1)} \quad (20)$$

Blasius correlation:

$$f = 0.079 Re^{-0.25} \quad (21)$$

where Pr is the Prandtl number, and where Re is the Reynolds number:

$$Pr = \frac{\mu C}{k} \quad (22)$$

$$Re = \frac{\dot{m} D_h}{A_c \mu} \quad (23)$$

$$D_h = \frac{4Wd}{2(W+d)} \quad (24)$$

W is the width of the area solar collector; d is the depth of the area solar collector. As suggested by [34], the convective heat transfer coefficient between the absorber plate and backplate was derived from Equation (25):

$$h_4 = Nu_m k_{fu} / D_e \quad (25)$$

Nu_m in Equation (26) is the Nusselt Number for the air moving through the packed bed, as defined by [35,36]:

$$Nu_m = 0.2 Re_m^{0.8} Pr^{1/3} \quad (26)$$

Re_m are the Reynolds numbers of the packed beds

$$Re_m = \dot{m}_f D_e / A_m \mu \quad (27)$$

The characteristic length D_e (m) of the porous materials is given by [37]:

$$D_e = \left(\frac{2}{3}\right) [\varepsilon D_m / (1 - \varepsilon)] \quad (28)$$

ε is the porosity of the packed bed from Equation (29):

$$\varepsilon = (V_1 - V_m) / V_1 \quad (29)$$

where V_1 is subjected to the total volume of the second air channel.

Meanwhile, the equivalent diameter D_m (m) of the bed is calculated from [37] and is calculated as per Equation (30):

$$D_m = 6V_s^{1/3} / n\pi \quad (30)$$

V_s is the total volume of n porous material particles, which is randomly selected.

The heat transfer area of the packed bed that is involved in the heat transfer A_m is also known as the wetted area and is given in Equation (31) [37]:

$$A_m = 6(1 - \varepsilon) / D_m \quad (31)$$

The convective heat transfer between h_3 and h_4 from absorber plate to the airflow in the second channel can be categorized as it was by [38]. As demonstrated in Equation (32),

the convective heat transfer coefficient $h_{\text{cpmf}2}$ lies between the packed bed, and the air flowing through the bottom channel is determined using the following correlation: [34]:

$$h_{\text{cpmf}2} = \left[\frac{1}{h_{\text{mf}}} + \frac{D_e}{S_m k_m} \right]^{-1} \quad (32)$$

where S_m is constant depending on the shape of the packed bed h_{mf} and can be calculated as:

$$h_{\text{mf}} = \text{Nu}_{\text{mf}} k_{\text{fu}} / D_e, \text{ with} \quad (33)$$

$$\text{Nu}_{\text{mf}} = \left(\frac{0.255}{\varepsilon} \right) \text{Re}_m^{\frac{2}{3}} \text{Pr}^{\frac{1}{3}} \quad (34)$$

Some of the physical properties of air were used along the collector to vary linearly with temperature, which was selected studies that have been previously published in the literature [39,40].

The thermal efficiency is considered to be a useful heat gain when solar radiation strikes the collector's surface. The formula is shown in Equation (35), according to [35,36]:

$$\eta_{\text{th}} = \frac{\dot{m} C_p (T_{\text{out}} - T_{\text{in}})}{A_c I} \quad (35)$$

where \dot{m} , C_p , T_{out} , T_{in} , A_c , and I are the mass flow rate, specific heat capacity, temperature out, the temperature in, area of collector, and solar irradiance, respectively. The pressure drop ΔP (N/m^2) in the air that is flowing in the smooth air channel, as stated in Equation (36), is the sum of the smooth channel friction loss ΔP_{smooth} and the dynamic loss due to the channel bends ΔP_{bend} [41]:

$$\Delta P_{\text{without packed bed}} = \Delta P_{\text{smooth}} + \Delta P_{\text{bend}} \quad (36)$$

$$\Delta P_{\text{smooth}} = 2\rho f V^2 L / D_h \quad (37)$$

$$\Delta P_{\text{bend}} = K\rho V^2 / 2 \quad (38)$$

$$V = \dot{m} / \rho W d_f \quad (39)$$

The value K for the 180° near reverse bend, as in the current system, is 2.2 [42]. For turbulent flow, the friction factor f is given by:

$$f = 0.059 \text{Re}^{-0.2} \quad (40)$$

The ΔP for the channel with the packing bed can be expressed by following Equation (41), as per [43]:

$$\Delta P_{\text{packed_bed}} = \left(2\rho f_m V^2 L \right) \frac{1 - \varepsilon}{\varepsilon^3} \quad (41)$$

where f_m denotes the friction factor for the packed bed channels, which is given as:

$$f_m = 150 \left[\frac{(1 - \varepsilon)}{\text{Re}_m} + 1.75 \right] \quad (42)$$

The Newton–Raphson iteration method was employed to numerically solve the energy balance equations in MATLAB. The use of this process has been published by [39,44], and the following process method is structured as in Figure 5.

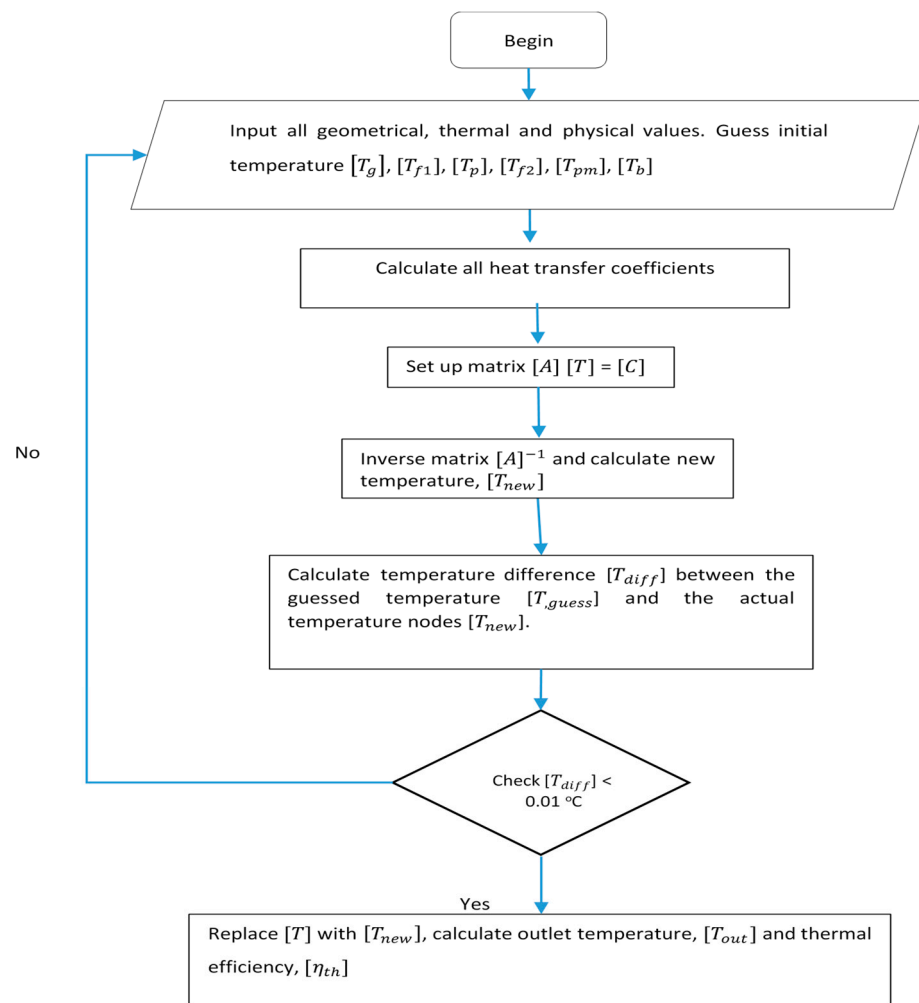


Figure 5. Computer iteration method using MATLAB.

2.3. Validation of the Mathematical Model

To validate the mathematical model, we compared the simulation results with an established experimental result by El-Sebaï et al. [45]. In achieving the aim, the design parameters in the mathematical model were matched with the designs, as they were in [45]. Comparisons between the theoretical and experimental by [45] are shown in Figure 6 to validate the theoretical model. Figure 6 indicates the effect of thermal efficiency in the DPSAH, with a mass flow rate range between 0.015 kg/s and 0.065 kg/s from the experimental results and from our simulation results. We can see that the trend of the theoretical curves is in good agreement with the experimental results of [45]. To further justify these findings, an error analysis using the root mean square percentage difference (RMSPD) and mean absolute percentage error (MAPE) were performed as they were by [46] and [47], respectively, the results of which are summarized in Table 4. The values of the accuracy measurements are considered acceptable, and this has been described in detail in [48].

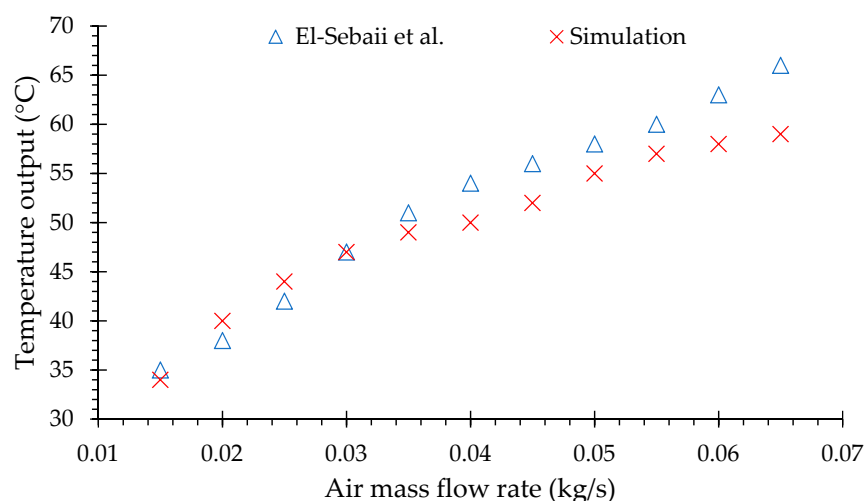


Figure 6. The Variation in the temperature output against the change in the mass flow rate: a comparison between the study of El-Sebaili et al. [45] and our simulation.

Table 4. The accuracy analysis of the theoretical model.

Parameter	T_{fo}
RMSPD	6.08%
MAPE	5.46%

3. Results and Discussion

The performance of the DPSAH with volcanic rock was investigated using the validated mathematical model. The optimum mass flow rate for the solar thermal collector was first determined. Then, the optimum porosity of the volcanic rock with the changes in mass flow rate was identified by considering the pressure drop in the solar collector. Finally, the potential of the DPSAH with volcanic rock for thermal storage applications was investigated by simulating the performance with the time of the day.

3.1. Determination of the Optimum Mass Flow Rate

To investigate the performance of the DPSAH with volcanic rock, the ambient temperature and the porosity of the packed bed were fixed at 30 °C and 85%, respectively. Meanwhile, the solar irradiance was set at 500, 600, 700, and 800 W/m², and the time for the simulation was averaged as 3600 s or 1 h. Figure 7 shows the variation in the thermal efficiency against the mass flow rate. The range of mass flow rate was between 0.015 kg/s and 0.065 kg/s. It can be observed that thermal efficiency increases as the mass flow rate increase, and increasing mass flow rate will increase the heat transfer rate in the DPSAH system. However, the change in the efficiency is not as significant as the increases that are seen in the radiation. The graphs show that the optimum mass flow rate that can be achieved at solar irradiance values ranging from 500 W/m² to 800 W/m² is 0.035 kg/s, with the average thermal efficiencies and fluid output temperatures ranging between 62% and 64% and from 41.7 °C to 48.3 °C, respectively.

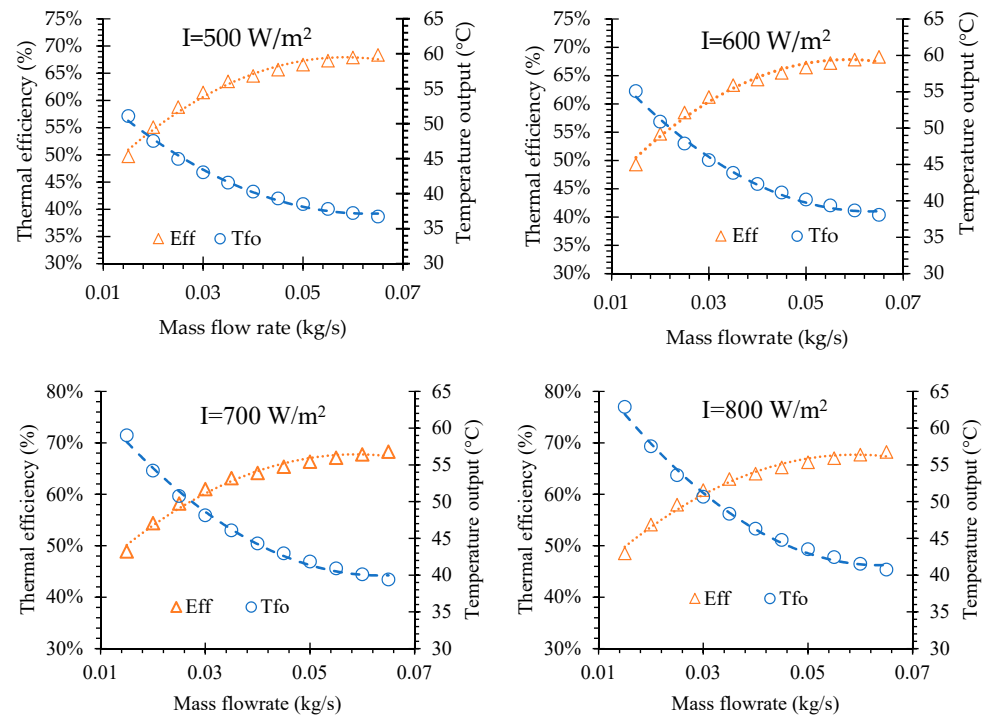


Figure 7. Thermal efficiency against output temperature at different irradiance.

3.2. Determination of the Optimum Porosity

On the other hand, the porosity of the packed bed materials (i.e., lava rock) was also investigated to determine its relationship with the performance of the collector. Referring to Equation (29), the porosity ϵ of the packed bed was varied by varying the total volume of the packed bed (i.e., lava rock). Nevertheless, it is crucial to note that using porous media in the DPSAH results in a friction effect for the airflow and hence a pressure drop. Excessive pressure drops lead to poor system performance due to the high amount of energy usage in the airflow. Pressure drop calculations were performed by employing Equations (36) and (41) to test the total airway pressure on the channel filled with porous media, as shown in Figure 8a with mass flow rate. It can be seen from the graph that the difference between the smooth channel and the packed bed is very noticeable. Changes in the pressure drop for the smooth ducts is less significant due to the minor frictional air contact, while more changes occur in the packed bed. It should also be noted that pressure increases slightly at lower mass flow level rates and then increases considerably afterward, as observed by Goyal et al. [49].

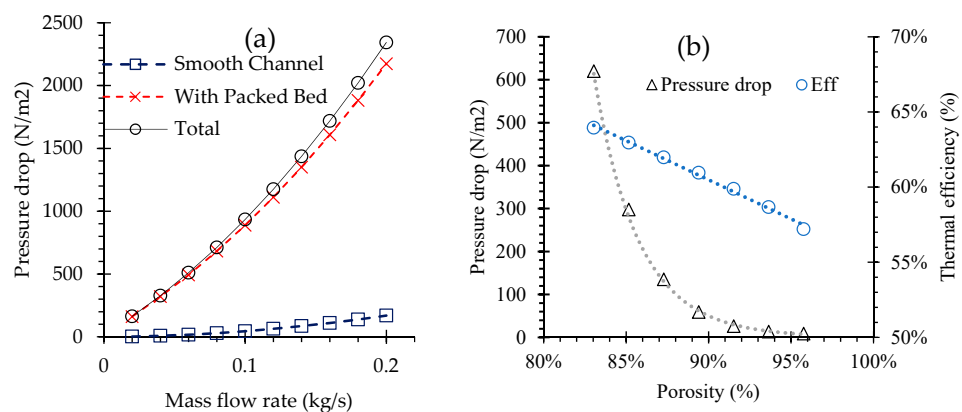


Figure 8. (a) Pressure drop against mass flow rate and (b) variation in thermal efficiency against the mass flow rate with different porosity values.

The optimum porosity of the packed bed materials is determined by considering both the pressure drop and the thermal efficiency of the collector. At an optimum mass flow rate of 0.035 kg/s, Figure 8b shows the variation in the thermal efficiency and pressure drop with different porosity values of 83%, 85%, 87%, 89%, 92%, 94%, and 96%. From Figure 8b, it can be concluded that decreasing the porosity can improve the efficiency; this is because the reduction in porosity can increase the heat transfer area per unit volume. This finding is in agreement from those in [11,50,51]. In addition, decreasing the porosity produces a larger surface area for heat transfer, and the higher volumetric heat-transfer coefficient greatly improved due to flowing air turbulence. However, the lower porosity results in a higher pressure drop that can be attributed to the increase in the friction factor in the air channel. Therefore, in this study, based on the analysis in Figure 8b, a porosity of 89% was selected.

3.3. The Variation with the Time of the Day

At the optimum porosity, the performance of the proposed DPSAH with lava rock as a packed bed material was investigated at different times of day on a typical sunny day in Kuala Lumpur, Malaysia. For solar irradiance between 500 W/m² to 1000 W/m², the mass flow rate was fixed at 0.035 kg/s. However, during low solar irradiance, the mass flow rate varied between 0.015 kg/s and 0.03 kg/s. The weather data were obtained from the "Meteonorm" directory in TRSNSYS 18. Figure 9 depicts substantial changes between the DPSAH with lava rock and with a conventional DPSAH. The time of day was divided into four parts: morning, peak time, evening, and when the sun had set. At the beginning of the graph, between 8:00 a.m. and 11:00 a.m., the increase in the output temperature on both systems proceeded at the same pace, but the DPSAH with lava rock shows a higher output temperature than conventional DPSAH. Figure 9 shows that the output temperature of the DPSAH with lava rock is 36 °C to 49 °C, whereas that for the conventional DPSAH ranges from 29 °C to 43 °C. However, the highest temperature was recorded between 11:00 a.m. and 4:00 p.m. during peak hours. The maximum output temperatures for the DPSAH with lava rock and for the conventional DPSAH were 54 °C and 48 °C, respectively. Both temperatures were taken at 1 p.m., when the solar irradiance reached a peak of 928 W/m². From 4 p.m. to 7 p.m., the output temperatures of both systems decreased substantially due to the drop in the solar irradiance. The reported output temperatures for the DPSAH with lava rock were 50 °C to 36 °C and from 44 °C to 28 °C for the conventional DPSAH as presented in Figure 9; beginning at 7 p.m. and with low to zero solar radiation, the output temperature for the conventional DPSAH drops and was found to be consistent with the variation in the ambient temperature. The presence of lava rock, on the other hand, shows higher values ranging from 31 °C to 35 °C compared to the conventional DPSAH, which provided values ranging from 24 °C to 28 °C, which occurred because the porous material retained heat due to its specific heat capacity. With this, the DPSAH with lava rock can be maintained at an acceptable temperature range for drying applications for a few hours during nighttime or at times when there is an absence of solar irradiance, hence extending its drying capacity period. Additionally, the average output temperatures of the DPSAH system with the lava rock and the conventional DPSAH overall were 47 °C and 40 °C, respectively. The computation yielded a 17.5% temperature difference between the two systems, implying a higher drying capacity for the DPSAH with lava rock than the conventional DPSAH.

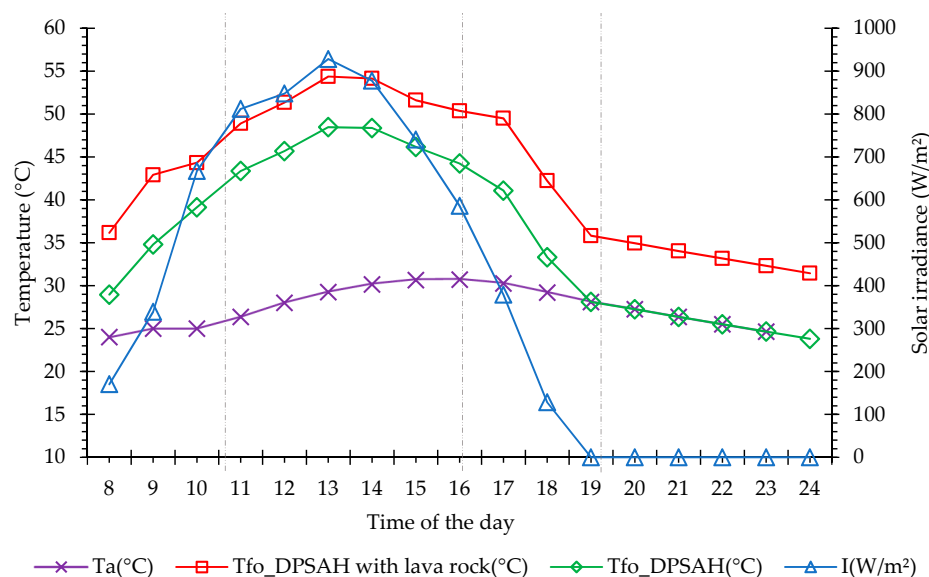


Figure 9. Solar Irradiance I, ambient temperature T_a , and air output temperature T_{fo} against the time of the day for the conventional double-pass solar air heater (DPSAH) and DPSAH with lava rock.

3.4. The Use of DPSAH with Lava Rock in Agricultural Drying

Using the DPSAH system in the drying of agricultural and food products can improve the quality through the production of a suitable output temperature in simulation studies. By maintaining an output temperature of about 40 °C to 50 °C with an appropriate mass flow rate, we can further diversify drying products and can be aware of external threats such as animals, insects, dirt, and dust. Table 5 shows some product materials from previous studies that can be used for drying applications using DPSAH systems.

Table 5. Dried products from selected studies.

Ref.	Sample	Temperature	Remark
[52]	Marine fish	45–50 °C	Products made at temperatures ranging from 45 °C to 50 °C were outstanding in taste, color, and texture.
[53]	Mint leaves	40–50 °C	Mass flow rate is set up between 0.01 kg/s to 0.05 kg/s.
[54]	Apple slices	20–50 °C	The thickness of the slice should be taken into account.
[55]	Cassava	40–50 °C	Temperatures higher than 80 °C may reduce the quality of the crop.
[56]	Unsalted and Salted catfish	50 °C	Drying for 8 h is recommended.
[57]	Red chili	28–55 °C	Maximum moisture content can be reduced to 10% within 33 h, maintaining an average drying temperature of about 44 °C.

4. Conclusions

The use of porous media in a DPSAH is constantly understudy and is involving to improve system performance. The use of lava rock in a DPSAH system was evaluated using energy balance in this study. Several findings have been achieved, including optimal efficiency, pressure drop, porosity, and differences between conventional and systems that have been analyzed against the time of day.

From the paper, the following conclusions can be made:

1. With the use of lava rock, the optimum thermal efficiency for the DPSAH that can be achieved ranges from 62% to 64% at a mass flow rate of 0.035 kg/s and at irradiances between 500 W/m² and 800 W/m²;

2. A porosity of 89% is the most suitable for considering the pressure drop and thermal efficiency trade-off;
3. The optimal temperature output range between 41.7 °C and 48.3 °C can be utilized to dry food, resulting in better food quality;
4. Compared to conventional double-pass solar air heaters (DPSAH), the overall temperature output of the DPSAH with lava rock is higher by approximately 17.5%;
5. The use of lava rock significantly impacts heat storage and can maintain continuous heat when employed for solar drying under the Malaysian climate.

This research serves as a starting platform for further research into DPSAHs with lava rock. The feasibilities of incorporating lava rock into DPSAHs have been proven based on the validated numerical model that was developed in this study. From the simulation, this study is attractive and promising. Experimental fabrication, testing, and collector optimization will be the focus of research in the future.

Author Contributions: Conceptualization, A.I., H.J. and K.S.; methodology, A.F.I., A.S.A.H. and A.I.; software, A.F.I., H.J. and A.I.; validation, A.I. and H.J.; formal analysis, A.F.I. and A.S.A.H.; investigation, A.I. and K.S.; resources, A.F.I., A.S.A.H. and A.I.; data curation, H.J.; writing—original draft preparation, A.F.I., A.I. and H.J.; writing—review and editing, A.F.I., H.J., A.I. and A.S.A.H.; visualization, K.S.; supervision, A.I. and K.S.; project administration, A.S.A.H., A.I. and K.S.; funding acquisition, A.S.A.H. All authors have read and agreed to the published version of the manuscript.

Funding: This research was funded by the Universiti Kebangsaan Malaysia (UKM), the Program Translational MRUN Rakan-RU-2019-001/4 research grant, and the Universiti Malaysia Sabah (UMS). The APC was funded by Universiti Malaysia Sabah (UMS).

Institutional Review Board Statement: Not applicable.

Informed Consent Statement: Not applicable.

Data Availability Statement: Not applicable.

Acknowledgments: The authors would like to thank the Solar Energy Research Institute, UKM and Faculty of Science and Natural Resources, UMS for the lab facilities.

Conflicts of Interest: The authors declare no conflict of interest.

Nomenclature

A_c	Area of solar collector (m^2)
A_{pm}	Area of porous (m^2)
A_m	Wetted area (m^2)
C	Specific heat capacity of fluid (J/kgK)
C_m	Specific heat capacity porous (J/kgK)
d	Collector depth (m)
D_m	The equivalent diameter of packed bed (m)
D_e	Characteristic length (m)
D_h	Equivalent diameter (m)
f	Friction factor
h	Heat-transfer coefficient (W/m^2K)
I	Irradiation (W/m^2)
k	Thermal conductivity (W/mK)
L	Length (m)
l	Thickness (m)
\dot{m}	Mass flow rate (kg/s)
M_m	Mass of porous (kg)
Nu	Nusselt number
r	Prandtl number
ΔP	Pressure drops (N/m^2)
Re	Reynold number

T	Temperature (°C)
U	Loss coefficient (W/m ² K)
v	Velocity (m/s)
V	Volume (m ³)
W	Collector width (m)
Subscripts	
a	Ambient
b	Backplate
f	Fluid
g	Glass
i	Inlet
m	Porous media
o	Outlet
p	Plate
pm	Porous media
r	Radiation
s	Sky
t	Top
th	Thermal
t	Insulation
w	Wind
1 and 2	Refer to the first and second stream of fluid
Greek	
α	Absorptivity
ε	Porosity
η	Efficiency
ρ	Density
τ	Transmissivity
δ	Thickness of porous
μ	Viscosity
σ	Stefan's Boltzmann constant

References

- Cassidy, V.M. Solar Collectors. In *Solar Heating and Cooling Systems*; Academic Press: Cambridge, MA, USA, 2017; Volume 46, pp. 29–97. [[CrossRef](#)]
- Hamid, A.S.A.; Ibrahim, A.; Mat, S.; Sopian, K. Experimental evaluation on large scale solar dryer for drying natural fiber in Malaysia. *Int. J. Renew. Energy Res.* **2019**, *9*, 598–604.
- Hamid, A.S.A.; Ibrahim, A.; Assadeg, J.; Ahmad, E.Z.; Sopian, K. Techno-economic Analysis of a Hybrid Solar Dryer with a Vacuum Tube Collector for Hibiscus Cannabinus L Fiber. *Int. J. Renew. Energy Res.* **2020**, *10*, 1609–1613.
- Ramani, B.M.; Gupta, A.; Kumar, R. Performance of a double pass solar air collector. *Sol. Energy* **2010**, *84*, 1929–1937. [[CrossRef](#)]
- Li, C.; Li, C.; Lyu, Y.; Qiu, Z. Performance of double-circulation water-flow window system as solar collector and indoor heating terminal. *Build. Simul.* **2020**, *13*, 575–584. [[CrossRef](#)]
- Belessiotis, V.; Delyannis, E. Solar drying. *Sol. Energy* **2011**, *85*, 1665–1691. [[CrossRef](#)]
- Lamrani, B.; Draoui, A.; Kuznik, F. Thermal performance and environmental assessment of a hybrid solar-electrical wood dryer integrated with Photovoltaic/Thermal air collector and heat recovery system. *Sol. Energy* **2021**, *221*, 60–74. [[CrossRef](#)]
- Luan, N.T.; Phu, N.M. First and second law evaluation of multipass flat-plate solar air collector and optimization using preference selection index method. *Math. Probl. Eng.* **2021**, *2021*, 5563882. [[CrossRef](#)]
- Mahmood, A.J.; Aldabbagh, L.B.Y.; Egelioglu, F. Investigation of single and double pass solar air heater with transverse fins and a package wire mesh layer. *Energy Convers. Manag.* **2015**, *89*, 599–607. [[CrossRef](#)]
- Alam, T.; Kim, M.H. Performance improvement of double-pass solar air heater—A state of art of review. *Renew. Sustain. Energy Rev.* **2017**, *79*, 779–793. [[CrossRef](#)]
- Sopian, K.; Alghoul, M.A.; Alfegi, E.M.; Sulaiman, M.Y.; Musa, E.A. Evaluation of thermal efficiency of double-pass solar collector with porous-nonporous media. *Renew. Energy* **2009**, *34*, 640–645. [[CrossRef](#)]
- Sopian, K.; Supranto; Daud, W.R.W.; Othman, M.Y.; Yatim, B. Thermal performance of the double-pass solar collector with and without porous media. *Renew. Energy* **1999**, *18*, 557–564. [[CrossRef](#)]

13. Aldabbagh, L.B.Y.; Egelioglu, F.; Ilkan, M. Single and double pass solar air heaters with wire mesh as packing bed. *Energy* **2010**, *35*, 3783–3787. [[CrossRef](#)]
14. Roy, A.; Hoque, E.; Islam, S.; Sarker, R.I.; Das, B.K. Efficiency Enhancement of Two Pass Solar Collectors with Steel Matrix in the Region of Rajshahi, Bangladesh. *Int. J. Mech. Eng. Autom.* **2017**, *4*, 71–76.
15. Ahmed, O.K.; Mohammed, Z.A. Influence of porous media on the performance of hybrid PV/Thermal collector. *Renew. Energy* **2017**, *112*, 378–387. [[CrossRef](#)]
16. Monem, M.A.; Akram, M.W.; Hossain, M.M.; Islam, M.R. Design and Performance Analysis of a Double Pass Solar Air Heater Using Black Coated Wire Mesh in Bangladesh Perspective. In Proceedings of the International Conference on Mechanical Engineering and Renewable Energy 2019 (ICMERE2019), Chittagong, Bangladesh, 11–13 December 2019; Volume 1, pp. 11–13.
17. Singh, S.; Dhruw, L.; Chander, S. Experimental investigation of a double pass converging finned wire mesh packed bed solar air heater. *J. Energy Storage* **2019**, *21*, 713–723. [[CrossRef](#)]
18. Velmurugan, P.; Kalaivanan, R. Energy and exergy analysis of solar air heaters with varied geometries. *Arab. J. Sci. Eng.* **2015**, *40*, 1173–1186. [[CrossRef](#)]
19. Dissa, A.O.; Ouoba, S.; Bathiebo, D.; Koulidiati, J. A study of a solar air collector with a mixed “porous” and “non-porous” composite absorber. *Sol. Energy* **2016**, *129*, 156–174. [[CrossRef](#)]
20. Singh, S.; Dhiman, P. Exergoeconomic analysis of recyctic packed bed solar air heater- sustained air heating system for buildings. *J. Energy Storage* **2016**, *5*, 33–47. [[CrossRef](#)]
21. Singh, S.; Dhiman, P. Analytical and experimental investigations of packed bed solar air heaters under the collective effect of recycle ratio and fractional mass flow rate. *J. Energy Storage* **2018**, *16*, 167–186. [[CrossRef](#)]
22. Hernández, A.L.; Quiñonez, J.E.; López, F.H. Transient numerical study of thermo-energetic performance of solar air heating collectors with metallic porous matrix. *Sol. Energy* **2019**, *178*, 181–192. [[CrossRef](#)]
23. Güler, H.Ö.; Sözen, A.; Tuncer, A.D.; Afshari, F.; Khanlari, A.; Şirin, C.; Gungor, A. Experimental and CFD survey of indirect solar dryer modified with low-cost iron mesh. *Sol. Energy* **2020**, *197*, 371–384. [[CrossRef](#)]
24. Singh, S. Experimental and numerical investigations of a single and double pass porous serpentine wavy wiremesh packed bed solar air heater. *Renew. Energy* **2020**, *145*, 1361–1387. [[CrossRef](#)]
25. Regar, L.; Amjad, A.I. Ancient Mineral Fibre for Green and Sustainable Development. *Tekstilec* **2016**, *59*, 321–334. [[CrossRef](#)]
26. Straaten, P.V. *Rocks for Crops: Agrominerals of Sub-Saharan Africa*; International Centre for Research in Agroforestry ICRAF: Nairobi, Kenya, 2002; p. 338. ISBN 0889555125.
27. Marty, J.; Ernst, G.G.J. *Volcanoes and the Environment*; Cambridge University Press: Cambridge, UK, 2005; ISBN 9780521592543.
28. Robertson, J.C.; Kerr, R.C. Solidification dynamics in channeled viscoplastic lava flows. *J. Geophys. Res. Solid Earth* **2012**, *117*. [[CrossRef](#)]
29. Watmuff, J.H.; Charters, W.W.S.; Proctor, D. Solar and wind induced external coefficients-solar collectors. *Coop. Mediterr. Energie Sol.* **1977**, *56*. Available online: https://www.researchgate.net/publication/234355019_Solar_and_wind_induced_external_coefficients_-_Solar_collectors (accessed on 1 November 2021).
30. Swinbank, W.C. Long-wave radiation from clear skies. *Q. J. R. Meteorol. Soc.* **1963**, *89*, 339–348. [[CrossRef](#)]
31. Heaton, H.S.; Reynolds, W.C.; Kays, W.M. Heat transfer in annular passages. Simultaneous development of velocity and temperature fields in laminar flow. *Int. J. Heat Mass Transf.* **1964**, *7*, 763–781. [[CrossRef](#)]
32. Gnielinski, V. New equations for heat and mass transfer in turbulent pipe and channel flow. *Int. Chem. Eng.* **1976**, *16*, 359–368.
33. Wang, C.; Gao, P.; Tan, S.; Wang, Z. Forced convection heat transfer and flow characteristics in laminar to turbulent transition region in rectangular channel. *Exp. Therm. Fluid Sci.* **2013**, *44*, 490–497. [[CrossRef](#)]
34. Dixon, A.G.; Cresswell, D.L. Theoretical prediction of effective heat transfer parameters in packed beds. *AIChE J.* **1979**, *25*, 663–676. [[CrossRef](#)]
35. Duffie, J.; Beckman, W.; Worek, W. *Solar Engineering of Thermal Processes*; John Wiley & Sons, Inc.: Hoboken, NJ, USA, 1994.
36. Beckman, W.A. *Solar Engineering of Thermal Processes*; John Wiley & Sons, Inc.: Hoboken, NJ, USA, 2013; ISBN 9780470873663.
37. Garg, H. *Advances in Solar Energy Technology: Volume 3 Heating, Agricultural and Photovoltaic Applications of Solar Energy*; Springer: New York, NY, USA, 2012.
38. Forson, F.K.; Nazha, M.A.A.; Rajakaruna, H. Experimental and simulation studies on a single pass, double duct solar air heater. *Energy Convers. Manag.* **2003**, *44*, 1209–1227. [[CrossRef](#)]
39. Ong, K.S. Thermal performance of solar air heaters: Mathematical model and solution procedure. *Sol. Energy* **1995**, *55*, 93–109. [[CrossRef](#)]
40. Fudholi, A.; Ruslan, M.H.; Othman, M.Y. Mathematical Model of Double-Pass Solar Air Collector. In *Latest Trends in Renewable Energy and Environmental Informatics*; WSEAS Press: Marathon, Greece, 2013; pp. 279–283.
41. White, F.M. *Fluid mechanics. McGraw-Hill Series in Mechanical Engineering*; McGraw-Hill Education: New York, NY, USA, 2011.
42. Daugherty, R.L. *Fluid Mechanics with Engineering Applications*; McGraw-Hill Education: New York, NY, USA, 1989; ISBN 1259002276.
43. Ergun, S. Fluid flow through packed columns. *Mater. Sci.* **1952**, *49*, 89–94.
44. Mustapha, M.; Fudholi, A.; Sopian, K. Mathematical modelling of bifacial photovoltaic-thermal (BPVT) collector with mirror reflector. *Int. J. Renew. Energy Res.* **2020**, *10*, 654–662.

45. El-Sebaei, A.A.; Aboul-Enein, S.; Ramadan, M.R.I.; El-Bialy, E. Year round performance of double pass solar air heater with packed bed. *Energy Convers. Manag.* **2007**, *48*, 990–1003. [[CrossRef](#)]
46. Dubey, S.; Tay, A.A.O. Testing of two different types of photovoltaic–thermal (PVT) modules with heat flow pattern under tropical climatic conditions. *Energy Sustain. Dev.* **2013**, *17*, 1–12. [[CrossRef](#)]
47. Sarhaddi, F.; Farahat, S.; Ajam, H.; Behzadmehr, A. Exergetic performance assessment of a solar photovoltaic thermal (PV/T) air collector. *Energy Build.* **2010**, *42*, 2184–2199. [[CrossRef](#)]
48. Jarimi, H.; Bakar, M.N.A.; Othman, M.; Din, M.H. Bi-fluid photovoltaic/thermal (PV/T) solar collector: Experimental validation of a 2-D theoretical model. *Renew. Energy* **2016**, *85*, 1052–1067. [[CrossRef](#)]
49. Goyal, R.K.; Tiwari, G.N.; Garg, H.P. Effect of thermal storage on the performance of an air collector: A periodic analysis. *Energy Convers. Manag.* **1998**, *39*, 193–202. [[CrossRef](#)]
50. Singh, S.; Dhiman, P. Using an analytical approach to investigate thermal performance of double-flow packed-bed solar air heaters with external recycle. *J. Energy Eng.* **2015**, *141*, 1–11. [[CrossRef](#)]
51. Jalil, J.M.; Ali, S.J. Thermal Investigations of Double Pass Solar Air Heater with Two Types of Porous Media of Different Thermal Conductivity. *Eng. Technol. J.* **2021**, *39*, 79–88. [[CrossRef](#)]
52. Reza, M.S.; Vapary, M.A.J.; Islam, M.N.; Kamal, M. Optimization of marine fish drying using solar tunnel dryer. *J. Food Process. Preserv.* **2009**, *33*, 47–59. [[CrossRef](#)]
53. Yusuf Sukman, J. Dried longtime in making herbal tea fragrant pandan leaves (*Pandanus amarylifolius* Roxb.) activities of antioxidant. *Вестник Росздравнадзора* **2017**, *4*, 9–15.
54. Blanco-Cano, L.; Soria-Verdugo, A.; Garcia-Gutierrez, L.M.; Ruiz-Rivas, U. Modeling the thin-layer drying process of Granny Smith apples: Application in an indirect solar dryer. *Appl. Therm. Eng.* **2016**, *108*, 1086–1094. [[CrossRef](#)]
55. Oestergaard Jensen, S.; Correll Frank, F.; Floejaard Kristensen, E. *Survey on Solar Dryers for Drying of Food and Wood in Ghana*; Danish Technological Institute: Taastrup, Denmark, 1999.
56. Mujaffar, S.; Sankat, C.K. Modeling the Drying Behavior of Unsalted and Salted Catfish (*Arius* sp.) Slabs. *J. Food Process. Preserv.* **2015**, *39*, 1385–1398. [[CrossRef](#)]
57. Fudholi, A.; Sopian, K.; Yazdi, M.H.; Ruslan, M.H.; Gabbasa, M.; Kazem, H.A. Performance analysis of solar drying system for red chili. *Sol. Energy* **2014**, *99*, 47–54. [[CrossRef](#)]